THE JOURNAL OF PHYSICAL CHEMISTRY C

Article

pubs.acs.org/JPCC

Thiadiazolo[3,4-*c*]pyridine Acceptor Based Blue Sensitizers for High Efficiency Dye-Sensitized Solar Cells

Jiangyi Mao,[†,‡] Jiabao Yang,[†,‡,§] Joël Teuscher,[§] Thomas Moehl,[§] Chenyi Yi,[§] Robin Humphry-Baker,[§] Pascal Comte,[§] Carole Grätzel,[§] Jianli Hua,*[,†] Shaik M. Zakeeruddin,*[,§] He Tian,[†] and Michael Grätzel*[,§]

[†]Key Laboratory for Advanced Materials and Institute of Fine Chemicals, East China University of Science and Technology, Shanghai 200237, People's Republic of China

[§]Laboratory for Photonics and Interfaces, Institute of Chemical Sciences and Engineering, Ecole Polytechnique Fédérale de Lausanne, CH-1015 Lausanne, Switzerland

ABSTRACT: Two new [1,2,5]thiadiazolo[3,4-*c*]pyridine-containing D-A-π−*A* organic dyes (**PT-1** and **PT-2**) have been designed and synthesized for utilization in dye-sensitized solar cells. **PT-2** sensitizer, which was synthesized by incorporating the 4,4-bis(2-ethylhexyl)-4*H*-cyclopenta[1,2-*b*:5,4-*b*′]dithiophene moiety as an additional π-bridge into the organic sensitizer **PT-1**, not only brings about significant changes in the absorption spectrum but also suppresses the charge recombination rate as compared to **PT-1**. Moreover, **PT-2** exhibits an aesthetic blue color covering a broad spectral range into the NIR region. The incident-photon to electron-conversion efficiency of **PT-2** shows an onset approaching 850 nm with power conversion efficiency of 6.7% fabricated when utilizing an iodide-based redox electrolyte. These results demonstrate that these [1,2,5]thiadiazolo[3,4-*c*]pyridine-based sensitizers are quite promising candidates to use for lowering the HOMO−LUMO gap and shifting the spectral response toward the NIR.

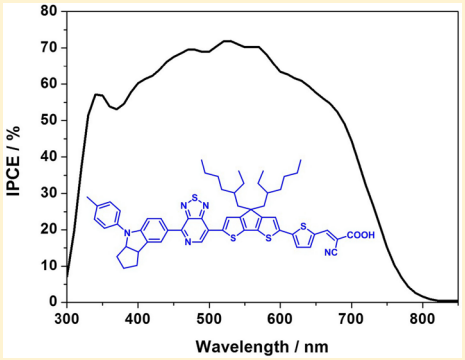

INTRODUCTION

Dye-sensitized mesoscopic solar cells (DSSCs) are efficient solar energy-to-electricity conversion devices and are one of the most promising next-generation renewable energy sources presently available due to their low material costs, flexibility, and easy manufacturing processes.[1,2] State of the art DSSCs that are based on organic dyes with a donor-π-bridge-acceptor (D-π-A) type configuration have recently achieved greater than 10% power conversion efficiency (PCE).[3−7] In order to reach a significant PCE, one of the requirements is that the sensitizer absorption spectra matches as closely as possible the solar emission spectrum in order to absorb the majority of available photons. In recent years researchers have focused on developing new dyes exhibiting a broad absorption spectra extending into the near-infrared (NIR) region. Blue-color squaraine,[8] phthalocyanine[9] and cyanine[10] dyes have been applied in DSSCs due to their intense absorption bands in the NIR region; however, the PCEs obtained were lower than 5.5%. One of the reasons for the lower performance observed is the narrow absorption band in the red/NIR region and no absorption in the high energy region below 550 nm.[11,12] In addition, both the formation of dye aggregates and the mismatch of energy levels for electron injection and/or dye regeneration play a decisive role.[13] Recently, a series of blue dyes with the diketopyrrolopyrrole (DPP) chromophore were synthesized for DSSCs. A maximum PCE of 7.1−7.7% was achieved using these chromophores in the presence of the iodine based redox system.[14] Thus, it is noteworthy to emphasize that, molecular engineering of NIR dyes is a high priority objective for obtaining superior photovoltaic performance.

The [1,2,5]thiadiazolo[3,4-*c*]pyridine (PT) hetero cycle has been employed in the construction of bulk-heterojunction solar cells utilizing low band gap copolymers and in solution-processed small-molecule solar cells due to its unique electron accepting properties.[15,16] The PT is a stronger acceptor compared to the benzothiadiazole (BTD) unit. One of the advantages of using PT in place of BTD is to shift the spectral response closer to the NIR. Second, the asymmetric nature of PT allows for monofunctionalization, resulting in facile and high synthetic yields. Recently, PT employed as an electron-deficient unit was utilized to synthesize panchromatic organic sensitizers for DSSCs, but the resulting PCEs were low.[17,18] Meanwhile, it has been found that the incorporation of additional electron-withdrawing units into the π bridge as internal acceptors, termed the D-A-π-A configuration, is beneficial for the tuning of the molecular energy levels and the red-shift of the charge-transfer absorption band, displaying distinct improvement in photovoltaic performance and stability. Cyclopentadithiophene (CPDT), emerged as an attractive

Special Issue: Michael Grätzel Festschrift

Received: February 2, 2014
Revised: April 4, 2014
Published: April 7, 2014

   dx.doi.org/10.1021/jp501173b | *J. Phys. Chem. C* 2014, 118, 17090−17099

building block for the development of photosensitizers due to its rigid conjugation structure and facile introduction of alkyl chains.[19] Organic dyes having alkyl-functionalized CPDT as the π-conjugated bridge are expected to exhibit improved optical properties, suppressed dye aggregation, and retarded charge recombination.[20,21] Herein, the PT unit (acting as an acceptor) and thiophene with/without 4,4-bis(2-ethylhexyl)-4*H*-cyclopenta[1,2-*b*:5,4-*b*′]dithiophene as the π-bridging molecule were incorporated into indoline based organic dyes (**PT-1** and **PT-2**, Figure 1). As expected, the two sensitizers exhibit

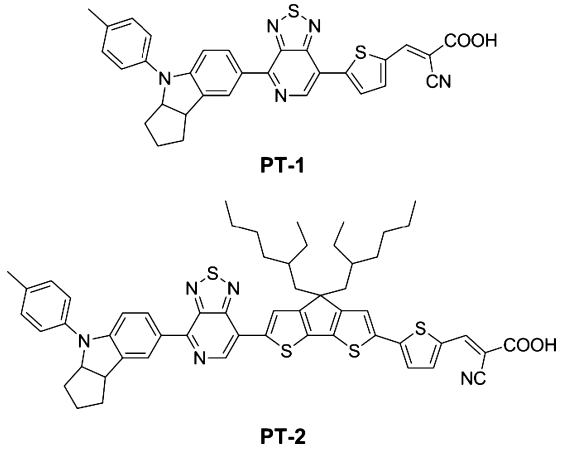

Figure 1. Molecular structures of the dyes **PT-1** and **PT-2**.

broadened absorption spectra, and the color of the **PT-2** dye is blue. Spectroscopic, electrochemical, and transient absorption studies of these sensitizers were undertaken to understand how structural modifications on the dyes affect the photovoltaic performance of DSSCs devices.

EXPERIMENTAL SECTION

Materials. Tetra-*n*-butylammonium hexafluorophosphate ($TBAPF_6$), 4-*tert*-butylpyridine (4-TBP), and lithium iodide were bought from Fluka and iodine, 99.999%, was purchased from Alfa Aesar. 5-Formyl-2-thiopheneboronic acid was bought from Sun Chemical Technology (Shanghai) Co., Ltd. The starting materials of 4,4-bis(2-ethylhexyl)-4*H*-cyclopenta[1,2-*b*:5,4-*b*′]dithiophene, 4,7-dibromo-[1,2,5]thiadiazolo[3,4-*c*]-pyridine and (4-(*p*-tolyl)-1,2,3,3a,4,8b-hexahydrocyclopenta[*b*]-indol-7-yl)boronic acid in Scheme 1 were synthesized according to refs 15, 20, and 22. Tetrahydrofuran (THF) was predried over 4 Å molecular sieves and distilled under an argon atmosphere from sodium benzophenoneketyl immediately prior to use. Dichloromethane (DCM) was distilled under normal pressure and dried over calcium hydroxide. All other chemicals were purchased from Aldrich and used as received without further purification.

Synthesis. *(4,4-Bis(2-ethylhexyl)-4H-cyclopenta[1,2-b:5,4-b′]dithiophen-2-yl)tributylstannane (**1**).* In a three-neck flame-dried round-bottom flask was dissolved 4,4-bis(2-ethylhexyl)-4*H*-cyclopenta[1,2-*b*:5,4-*b*′]dithiophene (800 mg, 2.0 mmol) in THF (20 mL) and cooled to −78 °C using a dry ethanol cold bath. Under argon, *n*-BuLi (1.5 mL, 1.6 M in hexanes, 2.4 mmol) was added dropwise to the reaction mixture, which was stirred for 3 h at −78 °C. After tributylstannyl chloride (800 mg, 2.4 mmol) was added in one portion via syringe, the mixture was slowly warmed up and stirred for 12 h at room temperature. Water was slowly added to terminate the reaction and the mixture was extracted three times with diethyl ether before the organic phase was washed with water and dried over anhydrous sodium sulfate. After solvent removal under reduced pressure, the crude product **1** was used to synthesize **4** without further purification.

*7-Bromo-4-(4-(p-tolyl)-1,2,3,3a,4,8b-hexahydrocyclopenta[b]indol-7-yl)-[1,2,5]thiadiazolo-[3,4-c]pyridine (**2**).* 4,7-Bibromo-[1,2,5]thiadiazolo[3,4-*c*]pyridine (300 mg, 1 mmol), $Pd(PPh_3)_4$ (100 mg, 0.09 mmol), and K_2CO_3 (1.00 g, 7.25 mmol) in 20 mL of THF and 5 mL of H_2O were heated to 55 °C under a nitrogen atmosphere for 30 min. A solution of (4-(*p*-tolyl)-1,2,3,3a,4,8b-hexahydrocyclopenta[*b*]indol-7-yl)boronic acid (300 mg, 1 mmol) in THF (5 mL) was added slowly, and the mixture was refluxed for further 6 h. After cooling to room temperature, the mixture was extracted with CH_2Cl_2 (3 × 30 mL). The organic portion was combined and dried over magnesium sulfate, then removed by rotary evaporation. The residue was purified by column chromatography (silica gel, dichloromethane/petroleum ether = 1/1) as eluent to yield a purple solid (170 mg, 36.8%). ^{1}H NMR (400 MHz, $CDCl_3$) δ 8.68 (s, 1H), 8.51−8.48 (m, 1H), 8.41 (s, 1H), 7.25−7.18 (m, 4H), 6.95 (d, J = 8.6 Hz, 1H), 4.91 (t, J = 7.3 Hz, 1H), 3.93 (t, J = 8.6 Hz, 1H), 2.36 (s, 3H), 2.14−2.08 (m, 1H), 2.03 (d, J = 3.5 Hz, 1H), 1.92 (s, 2H), 1.83−1.74 (m, 1H), 1.71−1.66 (m, 1H). ^{13}C NMR (100 MHz, $CDCl_3$) δ 153.46, 150.77, 144.48, 142.17, 140.10, 137.19, 134.60, 133.47, 131.24, 127.43, 124.84, 122.14, 118.78, 113.83, 108.98, 107.54, 95.08, 52.37, 46.19, 36.05, 34.64, 25.63, 21.62. MS (ES, m/z): $[M + H]^+$ calcd for $C_{23}H_{20}BrN_4S$, 463.1; found, 463.1.

*5-(4-(4-(p-Tolyl)-1,2,3,3a,4,8b-hexahydrocyclopenta[b]-indol-7-yl)-[1,2,5]thiadiazolo[3,4-c]pyridin-7-yl)thiophene-2-carbaldehyde (**3**).* Compound **2** (150 mg, 0.32 mmol), $Pd(PPh_3)_4$ (100 mg, 0.09 mmol) and K_2CO_3 (1.00 g, 7.25 mmol) in 20 mL of THF and 5 mL of H_2O were heated to 55 °C under a nitrogen atmosphere for 30 min. A solution of 5-formyl-2-thiopheneboronic acid (100 mg, 0.64 mmol) in THF (5 mL) was added slowly, and the mixture was refluxed for an additional 6 h. After cooling to room temperature, the mixture was extracted with CH_2Cl_2 (3 × 30 mL). The organic portion was combined and dried over magnesium sulfate, then removed by rotary evaporation. The residue was purified by column chromatography (silica gel, dichloromethane) as eluent to yield a purple solid (100 mg, 63.3%). ^{1}H NMR (400 MHz, $CDCl_3$) δ 8.85 (s, 1H), 8.59 (dd, J = 8.6, 1.7 Hz, 1H), 8.50 (s, 1H), 7.95 (d, J = 3.8 Hz, 1H), 7.27 (s, 2H), 7.23 (d, J = 8.4 Hz, 3H), 7.19 (d, J = 3.8 Hz, 1H), 7.02−6.99 (m, 1H), 4.97−4.93 (m, 1H), 3.81 (t, J = 6.7 Hz, 1H), 3.02 (d, J = 6.8 Hz, 3H), 2.20−2.08 (m, 2H), 1.86−1.77 (m, 2H), 1.76−1.68 (m, 2H). ^{13}C NMR (100 MHz, $CDCl_3$) δ 155.67, 149.65, 141.21, 139.30, 137.41, 135.74, 132.84, 131.36, 129.95, 127.39, 126.83, 126.4, 126.16, 121.48, 121.24, 118.05, 116.42, 107.02, 69.59, 45.20, 31.53, 29.72, 24.40, 20.92. MS (ES, m/z): $[M + H]^+$ calcd for $C_{28}H_{23}N_4OS_2$, 495.1; found, 495.1.

*7-(4,4-Bis(2-ethylhexyl)-4H-cyclopenta[1,2-b:5,4-b′]-dithiophen-2-yl)-4-(4-(p-tolyl)-1,2,3,3a,4,8b-hexahydrocyclopenta[b]indol-7-yl)-[1,2,5]thiadiazolo[3,4-c]-pyridine(**4**).* Compound **2** (150 mg, 0.32 mmol) and $Pd(PPh_3)_2Cl_2$ (100 mg, 0.14 mmol) in 20 mL of toluene were heated to 50 °C under a nitrogen atmosphere. After compound **1** (800 mg, 2.4 mmol) was added in one portion via syringe, the mixture was stirred for 3 h at 90 °C. The solvent was removed by rotary evaporation, and the crude reaction was

dx.doi.org/10.1021/jp501173b | J. Phys. Chem. C 2014, 118, 17090−17099

Scheme 1. Synthetic Route of PT-1 and PT-2

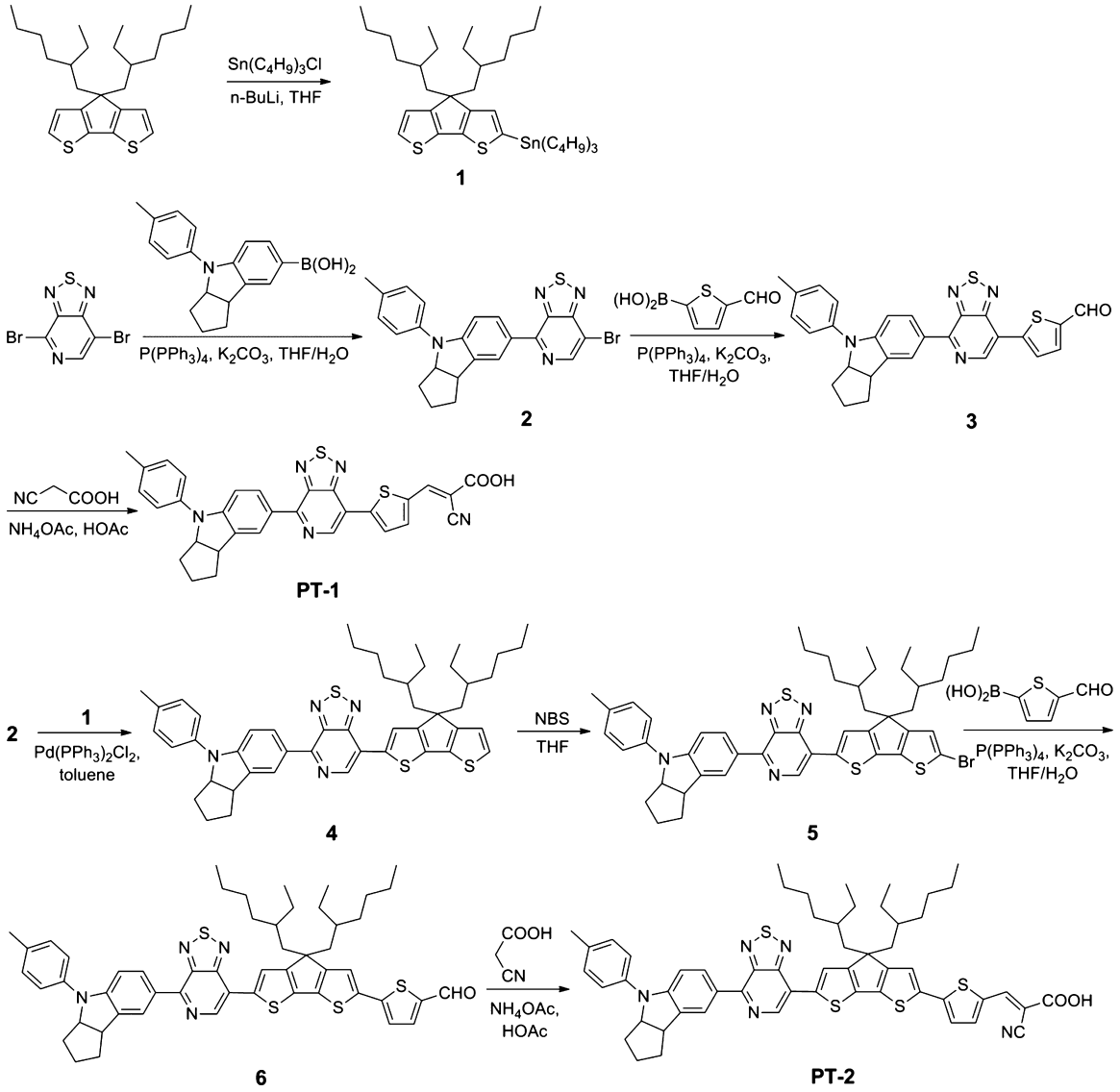

purified by column chromatography (dichloromethane/petroleum ether = 1/1) as eluent to yield a purple solid (200 mg, 80.0%). ^{1}H NMR (400 MHz, $CDCl_3$) δ 8.89−8.85 (m, 1H), 8.55 (dd, J = 8.6, 2.1 Hz, 1H), 8.46 (s, 1H), 8.02 (t, J = 7.5 Hz, 1H), 7.27 (d, J = 1.8 Hz, 1H), 7.25 (s, 1H), 7.22−7.18 (m, 3H), 7.02−6.96 (m, 2H), 4.91 (t, J = 6.7 Hz, 1H), 3.96 (t, J = 7.6 Hz, 1H), 2.36 (s, 3H), 2.02 (d, J = 8.8 Hz, 2H), 1.98−1.94 (m, 2H), 1.66−1.60 (m, 2H), 1.37 (t, J = 7.4 Hz, 4H), 1.01−0.95 (m, 10H), 0.92 (t, J = 7.3 Hz, 8H), 0.73−0.59 (m, 12H). ^{13}C NMR (100 MHz, $CDCl_3$) δ 159.65, 154.10, 151.19, 146.01, 140.37, 137.69, 136.60, 130.84, 128.18, 126.91, 126.37, 125.62, 124.87, 123.37, 122.00, 119.79, 117.09, 114.43, 113.68, 108.12, 54.80, 46.08, 44.42, 35.90, 32.30, 30.92, 30.01, 29.32, 28.06, 25.11, 23.58, 21.75, 14.33, 11.48, 11.36. MS (ES, m/z): $[M + H]^+$ calcd for $C_{48}H_{57}N_4S_3$, 785.3; found, 785.3.

*7-(6-Bromo-4,4-bis(2-ethylhexyl)-4H-cyclopenta[1,2-b:5,4-b′]dithiophen-2-yl)-4-(4-(p-tolyl)-1,2,3,3a,4,8b-hexahydrocyclopenta[b]indol-7-yl)-[1,2,5]thiadiazolo[3,4-c]-pyridine (**5**).* A solution of compound **4** (250 mg, 0.32 mmol) in THF (20 mL) was cooled to 0 °C. NBS (60 mg, 0.32 mmol) was added dropwise in one portion. The reaction mixture was stirred at 0 °C for 2 h. The reaction was quenched by addition of water and extracted with dichloromethane. The combined organic extract was dried over magnesium sulfate and filtered. Solvent removal by rotary evaporation and followed by column chromatography (silica gel, dichloromethane/petroleum ether = 1/2) as eluent to yield a purple solid (220 mg, 79.7%). ^{1}H NMR (400 MHz, $CDCl_3$) δ 8.82−8.78 (m, 1H), 8.69 (s, 1H), 8.36 (s, 1H), 7.96 (t, J = 7.1 Hz, 1H), 7.47 (d, J = 8.6 Hz, 1H), 7.29 (s, 1H), 7.09 (d, J = 8.1 Hz, 2H), 7.01 (d, J = 8.2 Hz, 2H), 4.44 (t, J = 6.5 Hz, 1H), 3.99 (t, J = 8.9 Hz, 1H), 2.30 (s, 3H), 2.07−1.98 (m, 2H), 1.92 (d, J = 4.8 Hz, 2H), 1.78 (d, J = 3.3 Hz, 3H), 1.12−1.01 (m, 6H), 0.88 (dd, J = 13.3, 7.0 Hz, 16H), 0.72 (d, J = 2.9 Hz, 3H), 0.57 (q, J = 7.5 Hz, 9H). ^{13}C NMR (100 MHz, $CDCl_3$) δ 156.15, 151.19, 149.11, 148.08, 143.52, 141.37, 139.61, 138.06, 135.92, 130.19, 127.61, 126.99, 126.26, 125.43, 124.60, 119.95, 119.28, 114.26, 105.70, 44.18, 36.17, 32.61, 32.13, 30.92, 30.43, 29.00, 27.50, 24.74, 23.37, 18.02, 14.80, 14.32, 12.22, 11.36. MS (ES, m/z): $[M + H]^+$ calcd for $C_{48}H_{56}N_4S_3$, 863.3; found, 863.3.

*5-(4,4-Bis(2-ethylhexyl)-6-(4-(4-(p-tolyl)-1,2,3,3a,4,8b-hexahydrocyclopenta[b]indol-7-yl)-[1,2,5]thiadiazolo[3,4-c]-pyridin-7-yl)-4H-cyclopenta[1,2-b:5,4-b′]dithiophen-2-yl)-thiophene-2-carbaldehyde (**6**).* Compound **5** (150 mg, 0.17

dx.doi.org/10.1021/jp501173b | J. Phys. Chem. C 2014, 118, 17090−17099

mmol), $Pd(PPh_3)_4$ (100 mg, 0.09 mmol), and K_2CO_3 (1.00 g, 7.25 mmol) in 20 mL of THF and 5 mL of H_2O were heated to 55 °C under a nitrogen atmosphere for 30 min. A solution of 5-formyl-2-thiopheneboronic acid (55 mg, 0.34 mmol) in THF (5 mL) was added slowly, and the mixture was refluxed for further 6 h. After cooling to room temperature, the mixture was extracted with CH_2Cl_2 (3 × 30 mL). The organic portion was combined and dried over magnesium sulfate, then removed by rotary evaporation. The residue was purified by column chromatography (silica gel, dichloromethane/petroleum ether = 2/1) as eluent to yield a purple solid (90 mg, 60.0%). ^{1}H NMR (400 MHz, $CDCl_3$) δ 9.88 (s, 1H), 9.21 (s, 1H), 8.99 (t, J = 2.3 Hz, 1H), 8.49 (s, 1H), 8.12−8.00 (m, 2H), 7.71 (dd, J = 3.9, 2.1 Hz, 1H), 7.39 (d, J = 8.2 Hz, 1H), 7.31 (d, J = 9.7 Hz, 2H), 7.27 (s, 2H), 7.23 (d, J = 8.5 Hz, 1H), 5.44 (d, J = 5.5 Hz, 1H), 4.74 (s, 1H), 2.59 (s, 3H), 2.39 (s, 1H), 2.26 (d, J = 7.5 Hz, 1H), 2.14 (d, J = 21.9 Hz, 2H), 1.82 (s, 2H), 1.32−1.23 (m, 6H), 1.07−0.98 (m, 16H), 0.75 (s, 3H), 0.67 (d, J = 6.7 Hz, 9H). ^{13}C NMR (100 MHz, $CDCl_3$) δ 163.23, 159.10, 155.91, 151.16, 148.67, 146.70, 142.19, 139.63, 137.14, 134.10, 132.43, 131.44, 128.72, 128.40, 128.02, 123.64, 123.19, 121.55, 121.08, 120.15, 117.26, 115.94, 115.07, 113.38, 111.58, 110.96, 109.39, 63.52, 61.93, 54.53, 49.37, 45.73, 43.15, 35.54, 27.53, 27.01, 23.04, 17.95, 14.45, 13.54, 10.94, 9.82. MS (ES, m/z): $[M + H]^+$ calcd for $C_{53}H_{59}N_4OS_4$, 895.4.3; found, 895.4.

*2-Cyano-3-(5-(4-(4-(p-tolyl)-1,2,3,3a,4,8b-hexahydrocyclopenta[b]indol-7-yl)-[1,2,5]thia- diazolo[3,4-c]pyridin-7-yl)thiophen-2-yl)acrylic acid (**PT-1**).* A mixture of aldehyde **3** (100 mg, 0.20 mmol) with cyanoacetic acid (50 mg, 0.60 mmol) in acetic acid (30 mL) was refluxed in the presence of ammonium acetate (100 mg, 1.30 mmol) for 6 h under argon. After cooling the solution, water was added to quench the reaction. The precipitate was filtered and washed with water. The residue was purified by column chromatography (silica gel, dichloromethane/EtOH = 15/1) as eluent to yield a purple solid (90 mg, 80.4%). ^{1}H NMR (400 MHz, DMSO-d_6) δ 9.03 (s, 1H), 8.54 (d, J = 8.7 Hz, 1H), 8.52 (s, 1H), 8.17 (d, J = 3.9 Hz, 1H), 8.15 (s, 1H), 7.82 (d, J = 4.1 Hz, 1H), 7.29 (d, J = 8.4 Hz, 2H), 7.23 (d, J = 8.4 Hz, 2H), 6.94 (d, J = 8.6 Hz, 1H), 5.02−4.98 (m, 1H), 3.92 (t, J = 7.8 Hz, 1H), 2.32 (s, 3H), 2.10 (dd, J = 16.3, 9.6 Hz, 2H), 1.82 (dd, J = 12.8, 6.1 Hz, 2H), 1.70−1.61 (m, 2H). ^{13}C NMR (100 MHz, DMSO-d_6) δ 181.26, 164.63, 162.41, 149.84, 149.27, 148.16, 141.66, 135.55, 132.37, 131.13, 128.24, 128.11, 122.41, 107.45, 100.55, 97.36, 74.22, 70.18, 64.06, 50.65, 45.51, 21.82. HRMS (ESI, m/z): $[M - H]^-$ calcd for $C_{31}H_{22}N_5O_2S_2$, 560.1215; found, 560.1216.

*3-(5-(4,4-Bis(2-ethylhexyl)-6-(4-(4-(p-tolyl)-1,2,3,3a,4,8b-hexahydrocyclopenta[b]indol-7-yl)-[1,2,5]thiadiazolo[3,4-c]-pyridin-7-yl)-4H-cyclopenta[1,2-b:5,4-b′]dithiophen-2-yl)-thiophen-2-yl)-2-cyanoacrylic acid (**PT-2**).* The synthesis method resembles that of compound **PT-1**, and the compound was purified by column chromatography (silica gel, dichloromethane/EtOH = 15/1) as eluent to yield a blue solid (80 mg, 69.6%). ^{1}H NMR (400 MHz, DMSO-d_6) δ 9.15 (s, 1H), 9.04 (s, 1H), 8.46 (d, J = 12.0 Hz, 1H), 8.32 (t, J = 5.9 Hz, 1H), 8.09 (s, 1H), 7.98 (s, 1H), 7.66−7.62 (m, 2H), 7.49 (d, J = 8.2 Hz, 1H), 7.39 (dd, J = 13.9, 9.1 Hz, 2H), 7.29 (d, J = 9.4 Hz, 1H), 7.22 (d, J = 8.3 Hz, 1H), 4.97 (s, 1H), 3.89 (s, 1H), 2.31 (s, 1H), 2.07 (s, 3H), 1.80 (s, 1H), 1.30 (s, 2H), 1.26 (s, 2H), 1.23 (s, 6H), 0.98 (dd, J = 18.2, 13.1 Hz, 16H), 0.69−0.67 (m, 3H), 0.66−0.58 (m, 9H). ^{13}C NMR (100 MHz, DMSO-d_6) δ 181.45, 174.30, 163.94, 161.35, 153.97, 142.45, 136.18, 135.10, 131.99, 130.67, 128.69, 128.38, 127.05, 126.78, 125.33, 124.13, 123.47, 119.25, 118.63, 118.31, 117.89, 116.83, 116.06, 114.88, 112.08, 110.14, 96.34, 69.96, 66.42, 54.12, 50.15, 45.80, 43.06, 39.65, 34.50, 28.43, 26.48, 22.14, 20.09, 16.63, 12.53, 11.39. HRMS (ESI, m/z): $[M - H]^-$ calcd for $C_{56}H_{58}N_5O_2S_4$, 960.3473; found, 960.3480.

Cell Fabrication. DSSCs were fabricated by using a previously reported procedure and consist of a dye-sensitized double-layered photoanode made of mesoporous TiO_2, an appropriate electrolyte and a counter electrode.[23,24] A transparent, 8 μm thick layer of 20 nm particles was screen-printed onto a FTO glass pane (NSG-10, Nippon Sheet Glass), pretreated with $TiCl_4$. Subsequently, a 5 μm thick layer of scattering particles (300 nm diameter) was screen-printed, and the thus formed electrode was sintered by ramping to 500 °C. The $TiCl_4$ post-treatment was performed on the substrates in order to increase the surface area. The photoanodes were sintered once again and after cooling down to 80 °C, were immersed in a 0.1 mM dye bath with CDCA in a chloroform and ethanol (v/v, 3/7) mixed solution for 4 h at room temperature. The electrode was then rinsed with CH_3CN and dried. After rinsing with the same solvent, the stained substrates were sealed with pieces of thermally platinized (a drop of 8 mM hexachloroplatinic solution in 2-propanol, heated to 425 °C) FTO glass (TEC15, Pilkington), which served as a counter electrode. The 25 μm thick Surlyn (Dupont) was used as a binder and a spacer. The electrolytes were introduced into the cells via predrilled holes in the counter electrodes.

DSSCs Characterization. A 450 W xenon light source (Oriel, U.S.A.) was used to characterize the solar cells. The spectral output of the lamp was matched in the region of 350−750 nm with the aid of a Schott K113 Tempax sunlight filter (PräzisionsGlas&Optik GmbH, Germany) so as to reduce the mismatch between the simulated and true solar spectra to less than 4%. The current−voltage characteristics of the cell, under these experimental conditions, were obtained by applying an external potential bias to the cell and measuring the generated photocurrent with a Keithley model 2400 digital source meter (Keithley, U.S.A.). For IPCE measurements, a modulated light intensity data acquisition system was used to control the incident photon-to-current conversion efficiency (IPCE) measurement. The modulation frequency was about 1 Hz. Light from a 300 W xenon lamp (ILC Technology, U.S.A.) was focused through a computer controlled Gemini-180 double monochromator (JobinYvon Ltd., U.K.) onto the photovoltaic cell under test. A white light bias was used to bring the total light intensity on the device under test closer to operating conditions. The devices were masked with a black metal aperture to attain an illuminated active area of 0.159 cm^2.

Photoinduced Absorption Spectroscopy (PIA). PIA spectra were recorded over 500−1100 nm on transparent devices containing I^-/I_3^- electrolyte and an 8 μm TiO_2 film loaded with dyes **PT-1** or **PT-2**. The samples were excited with a 470 nm LED, modulated at 9 Hz (square wave), and driven by the detection lock-in amplifier. White light from a halogen bulb was used as a probe. These spectra allowed identification of the position of oxidized dye species.

Transient Absorption Spectroscopy (TAS). Nanosecond laser flash photolysis was applied to samples loaded with dyes **PT-1** or **PT-2** (identical to PIA samples). The samples were excited by 7 ns (fwmh) pulsed laser light produced at a repetition rate of 20 Hz by an optical parametric oscillator pumped by a frequency-tripled Qswitched Nd:YAG laser. The output excitation wavelength was tuned to 605 nm, and the

laser fluence on the sample was kept at a low level (50 μJ cm^{-2} per pulse) to ensure that, on average, less than one electron is injected per TiO_2 nanoparticle per pulse. The probe light consists of a xenon arc lamp passed through a 665 nm cutoff filter and a water filter, focused onto the sample and collected in a monochromator at 750 nm. The detector is a fast photomultiplier tube connected to a digital oscilloscope. Typical data are averaged over 1000 laser shots and smoothed using a Savitzky-Golay filter. The transient absorption measurements were performed on the previously described dye-sensitized, 4 μm thick, transparent TiO_2 photoanode either coated with a drop of 3-methylproprionitrile or with the Z960 electrolyte to inhibit degradation. The composition of Z960 is 1.0 M 1,3-dimethylimidazolium iodide, 0.03 M I_2, 0.05 M lithium iodide, 0.1 M guanidiniumthiocyanate, and 0.5 M *tert*-butylpyridine in acetonitrile and valeronitrile solvent mixture (85:15, v/v).

Electrochemical Impedance Spectroscopy (EIS). The EIS analysis was done on DSSC devices at a constant temperature of 20 °C in the dark. A sinusoidal potential perturbation with an amplitude of 15 mV was applied over a frequency range of 7 MHz to 0.1 Hz (Bio Logic SP300 potentiostat) at constant potential bias. The bias potential varied between 0 mV and V_{oc} in about 50 mV incremental steps. The spectra were fitted using ZView software (Scribner Associates) applying the transmission line model.[25,26] If the potential was corrected for the ohmic losses due to the series resistance of the devices, it is indicated in the figure caption.

RESULTS AND DISCUSSION

Synthesis of Sensitizers. Scheme 1 illustrates the synthetic protocol for the organic dyes **PT-1** and **PT-2**. Two steps of Suzuki coupling reactions on 4,7-bibromo-[1,2,5]thiadiazolo-[3,4-*c*]pyridine resulted in the corresponding aldehyde precursor **3**, followed by treatment with cyanoacetic acid under typical Knoevenagel condensation to obtain the target dye **PT-1**. Compound **4** was synthesized by a step of Suzuki coupling reaction and a subsequent Stille coupling reaction, followed by NBS addition to give **5**. The synthetic method of **PT-2** dye is similar to **PT-1**. In the Suzuki coupling reaction, preferential oxidative coupling occurs at the more electron deficient 4-carbon position of pyridine derivative leading to the pyridyl N atoms proximal to the donor.[27] It is important to highlight the regioselective chemistry of **2**, where the pyridyl N atoms of the PT acceptor unit are oriented toward the indoline donor moiety (proximal configuration).[28] Bromo-substituted indoline is extremely photosensitive due to it slow oxidation potential.[29] In contrast, the intermediate **2** is photostable even when a **PT** unit is attached. Incorporation of a strong electron-withdrawing unit such as PT undoubtedly increases the photostability of **2** due to the favorable electron distribution within the donor section.

Spectroscopic Studies. Figure 2a shows the UV−visible absorption and emission spectra of **PT-1** and **PT-2** dyes in $CHCl_3$ solution. The absorption peaks as well as their molar extinction coefficients are summarized in Table 1. The low energy absorption maxima of the two dyes exhibited at 576 nm (ε = 3.58 × 10^4 M^{-1} cm^{-1}) and 593 nm (ε = 3.37 × 10^4 M^{-1} cm^{-1}), respectively, are due to the intramolecular charge transfer (ICT) transition from the indoline donor group to the cyanoacrylic acid acceptor unit. When compared to the reference dye, **WS-2**, that has a BTD unit as acceptor,[29] the introduction of the more efficient electron acceptor PT unit into the molecular frame further decreases the gap between the highest occupied molecular orbital (HOMO) and the lowest unoccupied molecular orbital (LUMO), thus, shifting the ICT absorption peak from 533 nm (**WS-2**) to 576 nm (**PT-1**). The **PT-2** dye was synthesized by the insertion of 4,4-bis(2-ethylhexyl)-4*H*-cyclopenta[1,2-*b*:5,4-*b*′]dithiophene as a π-conjugated spacer into **PT-1**. The low energy absorption maximum of **PT-2** has a 17 nm redshift compared to **PT-1**, but there is no apparent red shift in the absorption threshold, which is around 680 nm. As we all know, the longer wavelength absorption region is assigned to the ICT transition from the donor to acceptor segments, while the shorter wavelength region is attributed to the $\pi \rightarrow \pi^*$ transition of the donor. Since the two compounds have common indoline donor and

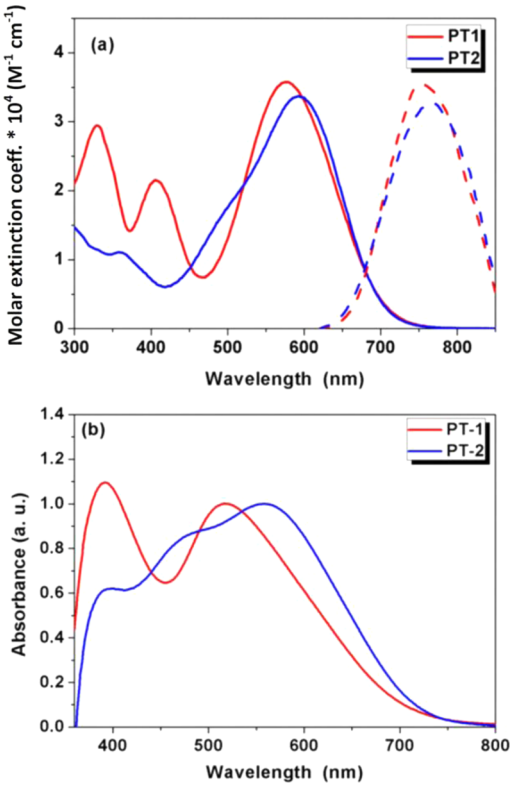

Figure 2. (a) UV−vis absorption and emission spectra of **PT-1** and **PT-2** in $CHCl_3$ solution and (b) UV−vis absorption spectra of **PT-1** and **PT-2** adsorbed on transparent TiO_2 films.

Table 1. Optical Properties and Electrochemical Properties of the Dyes PT-1 and PT-2

dye	$\lambda_{abs,max}$[a] (nm; ε × 10^4 M^{-1} cm^{-1})	$\lambda_{em,max}$[b] (nm)	$\lambda_{abs,max}$[c] (nm)	E^0_{ox}[d]/V (vs NHE)	E_{0-0}[e] (eV)	Φ^0 (S^+/S^*)[f]/V (vs NHE)
PT-1	576 (3.58)	752	516	0.89	1.82	−0.93
PT-2	593 (3.37)	766	558	0.88	1.83	−0.95

[a]Absorption maximum in $CHCl_3$ solution (1.5 × 10^{-5} M). [b]Emission maximum in $CHCl_3$ solution (excited at 600 nm). [c]Absorption maximum on 4 μm TiO_2 transparent films. [d]Redox potentials were measured in CH_2Cl_2 with 0.1 M tetra-*n*-butylammonium hexafluorophosphate ($TBAPF_6$) as electrolyte (working electrode, Pt; reference electrode, SCE, calibrated with ferrocene/ferrocenium (Fc/Fc^+) as an external reference and converted to NHE by addition of 0.69 V; counter electrode, Pt). [e]E_{0-0} was calculated from the absorption and emission spectra of the dyes. [f]$\Phi^0(S^+/S^*)$ is estimated by subtracting E_{0-0} from E^0_{ox}.

dx.doi.org/10.1021/jp501173b | J. Phys. Chem. C 2014, 118, 17090−17099

cyanoacrylic acid acceptor, the changes in their absorption behaviors are ascribed to the alkyl cyclopentadithiophene (CPDT) spacer segments. However, the CPDT group with two alkyl chains has bulky steric hindrance; this may influence the conjugation of the dye. So, the absorption thresholds from UV−vis absorption spectra of the two dyes does not change much. The absorption maxima of **PT-1** and **PT-2** dyes adsorbed on the 4 μm transparent TiO_2 films are blue-shifted to 516 and 558 nm, respectively. The blue shift in the absorption spectra of dyes adsorbed on the surface of the TiO_2 film may be ascribed to the deprotonation of the carboxylic acid.[30−32]

The redox potentials of **PT-1** and **PT-2** sensitizers were scrutinized by cyclic voltammetry in CH_2Cl_2 solvent containing 1.0 M tetra-*n*-butylammonium hexafluorophosphate. Sensitizer-stained TiO_2 film was used as the working electrode, and it shows a quasi-reversible couple. The measured redox potentials are collected in Table 1. The redox potentials of **PT-1** and **PT-2** were measured to be 0.89 and 0.88 V versus NHE, respectively. The redox potentials of both the dyes show similar values, as they have the same electron donor group, indoline. The redox potentials are more positive than that of I^-/I_3^- redox couple, suggesting sufficient driving force for dye regeneration. The band gap energies (E_{0-0}) of the dyes are 1.82 and 1.83 eV, respectively, which were estimated from the absorption and emission spectra of the dyes. The estimated excited-state potentials for **PT-1** and **PT-2** calculated from $\Phi^0(S^+/S^*) - E_{0-0}$, are −0.93 and −0.95 V, respectively. The excited state reduction potentials of these dyes are sufficiently more negative than the TiO_2 conduction band edge energy level (−0.5 V vs NHE) to make the electron injection process efficient.

DFT Calculations. To gain insight into the molecular structure and electron distributions, density functional theory (DFT) calculations were performed at the B3LYP/6-31G* level of theory with Spartan 14.[33] The electron distributions within the HOMO and LUMO levels of the dyes are shown in Figure 3. In the **PT-1** and **PT-2** dyes the HOMO levels are

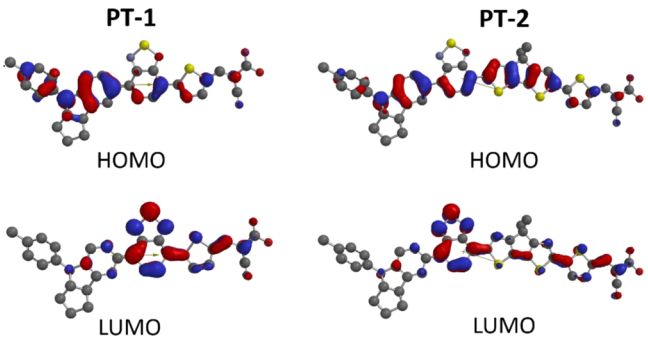

Figure 3. Calculated HOMOs and LUMOs of **PT-1** and **PT-2**.

mainly localized on the donor and PT unit, while the LUMO levels have a π-orbital delocalization throughout the PT and the 2-cyanoacrylic acid moieties.

Photovoltaic Performance. The photocurrent density voltage curves ($J-V$) and the incident photon to current conversion efficiency (IPCE) spectra of the DSSCs based on the **PT-1** and **PT-2** dyes are shown in Figure 4. Photovoltaic parameters such as short-circuit current density (J_{sc}), open-circuit voltage (V_{oc}), fill factor (FF), and power conversion efficiency (PCE) are collected in Table 2. A total of 2 mM

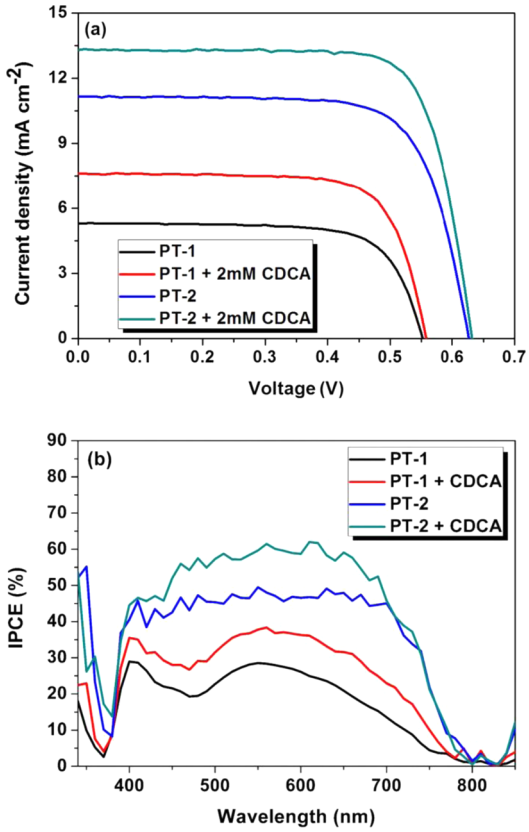

Figure 4. (a) Current−voltage characteristics of DSSCs based on **PT-1** and **PT-2** and (b) IPCE action spectra for DSSCs based on **PT-1** and **PT-2** with and without CDCA.

Table 2. Photovoltaic Performance of the Dyes[a]

dye	CDCA (mM)	J_{sc} (mA cm^{-2})	V_{oc} (mV)	FF	η (%)
PT-1	0	5.3	552	0.72	2.1
	2	7.6	557	0.73	3.1
PT-2	0	11.2	626	0.72	5.1
	2	13.3	631	0.76	6.4

[a]Electrolyte: 0.03 M I_2, 0.05 M LiI, 0.5 M TBP, 0.1 M GNCS, 1.0 M DMII in acetonitrile and valeronitrile (v/v, 85/15).

chenodeoxycholic acid (CDCA) was added as coadsorbent into the dye solution to avoid dye aggregation. The $J-V$ curves of DSSCs in the presence and absence of CDCA are shown in Figure 4. As shown, CDCA has an influence in augmenting photovoltaic performance in the presence of both dyes through an enhancement in the J_{sc} values. For **PT-1**, CDCA increases the photovoltaic performance significantly: J_{sc} augments from 5.3 to 7.6 mA cm^{-2}, and the power conversion efficiency improves from 2.1% to 3.1%. For **PT-2**, J_{sc} augments from 11.2 to 13.3 mA cm^{-2}, and the power conversion efficiency improves from 5.1% to 6.4%. The significant increase in J_{sc} following CDCA coadsorption for both of the dyes can be explained by a decrease in aggregation since there is an observed increase in magnitude in the IPCE (Figure 3b).

The composition of the redox electrolyte also plays a significant role on the DSSC's device performance. The position of the TiO_2 conduction band (CB) depends on the surface charge, which is influenced by the electrolyte composition. Presence of Li^+ ions in the redox electrolyte shifts the conduction band edge of TiO_2 to the positive side

dx.doi.org/10.1021/jp501173b | J. Phys. Chem. C 2014, 118, 17090−17099

due to the adsorption of Li^+ ions at the TiO_2/electrolyte interface. Presence of negatively charged ions or Lewis base molecules, such as 4-TBP, shifts the CB edge to more negative potentials.[34] Hence, depending on the composition of the electrolyte the photovoltaic performance of DSSC devices varies. As the PV performance of **PT-2** devices is higher than those made with **PT-1**, we selected **PT-2** to test with I^-/I_3^- electrolyte containing different additives. Figure 5 exhibits the

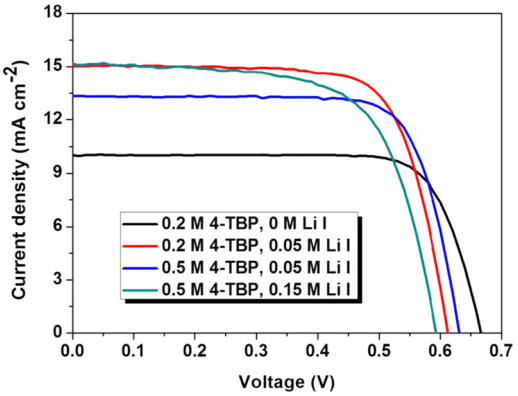

Figure 5. Current−voltage characteristics of **PT-2**-based DSSCs with different additives in the electrolyte.

$J-V$ curves, and the corresponding photovoltaic data are collected in Table 3. As expected, increasing Li^+ concentration

Table 3. Photovoltaic Performance of DSSCs with Different Additives in the Electrolyte

dye	4-TBP (M)	LiI (M)	J_{sc} (mA cm^{-2})	V_{oc} (mV)	FF	η (%)
PT-1	0.2	0.05	9.2	543	0.72	3.6
PT-2	0.2	0	10.0	666	0.76	5.1
	0.2	0.05	15.1	612	0.72	6.7
	0.5	0.05	13.3	631	0.76	6.4
	0.5	0.15	15.2	593	0.66	5.9

leads to an increase in J_{sc} and a drop in the V_{oc} values due to a positive shift of the TiO_2 conduction band.[35] Addition of 4-TBP leads to a negative shift of the TiO_2 conduction band edge resulting in a decrease of the electron injection rate constant and the injection efficiency.[34] Consequently, the V_{oc} increases from 612 mV to 631 mV, but the J_{sc} decreases from 15.1 mA to 13.3 mA. The optimal composition of electrolyte for higher **PT-2** device performance is 0.2 M 4-TBP and 0.05 M Li^+ in the I^-/I_3^- electrolyte where a PCE of 6.7% was achieved. Using the same electrolyte, the **PT-1**-based DSSC device's PCE reached 3.6% (see Table 3).

Electrochemical impedance spectroscopy, photoinduced absorption spectroscopy, and transient absorbance spectroscopy studies were undertaken to understand how structural modifications on dyes influence the photovoltaic parameters of the DSSCs devices.

Electrochemical impedance spectroscopy. Electrochemical impedance spectroscopy (EIS) measurements give a direct access to the charge transfer resistance of the TiO_2/dye/electrolyte interface. EIS investigations were performed in the dark on devices with **PT-1** and **PT-2** dyes containing optimized electrolyte (0.2 M TBP, 0.05 LiI) to understand in more detail the electronic properties of the devices. The EIS measurements were fitted according to the transmission line model.[25,26] The charge transfer resistance, R_{ct}, representing the charge transfer between electrons from the FTO substrate (low forward bias) or the mesoporous TiO_2 (high forward bias) with the oxidized form of the redox couple in the electrolyte, mirrors nicely the behavior of the dark current versus voltage behavior of the devices (see Figure 6 and the inset).

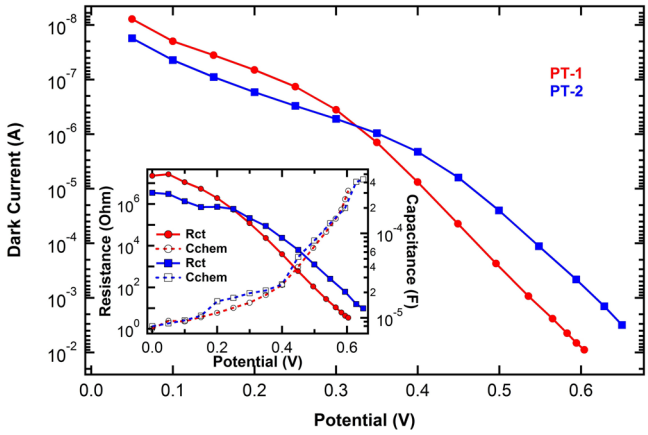

Figure 6. Dark current−voltage characteristics of **PT-1** and **PT-2** based DSSCs during the EIS measurement. Inset shows the results for the R_{ct} and chemical capacitance C_{chem} of these devices plotted against applied potential (forward bias). The plotted potential is corrected for the IR drop due to the series resistance.

From the EIS results one can determine the DOS (density of states) of the mesoporous TiO_2 as well as the electron lifetime ($\tau_n = R_{ct} \times C_{chem}$). The DOS is defined as

$$\mathrm{DOS} = \frac{C_{chem}}{qAL(1-p)}$$

where q represents the elementary charge, A the geometric area of the cell, and p the film porosity. The DOS thus determined indicates no change in the distribution of trap states for the two different devices as well as a similar conduction band position of the mesoporous TiO_2 (see insets in Figures 6 and 7). Plotting the electron lifetime against the DOS shows, as do the plots of the charge transfer resistance versus bias, a longer lifetime, or slower recombination, for **PT-2** compared to **PT-1**. The longer τ_n in the presence of **PT-2** leads to the higher observed photovoltage in the device. A rough estimation of the difference in final V_{oc} of the devices can be drawn from the

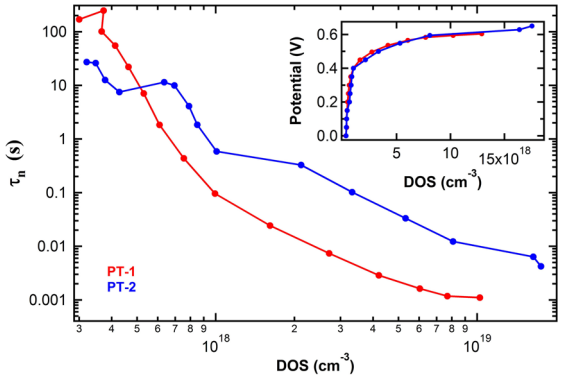

Figure 7. Electron lifetime plotted vs DOS. Inset shows the IR Drop corrected applied potential against the DOS.

dx.doi.org/10.1021/jp501173b | J. Phys. Chem. C 2014, 118, 17090−17099

diode equation ($\Delta V_{oc} = (k_B T/q)\ln(\tau_{n1}/\tau_{n2})$ with k_B as Boltzmann constant, T as temperature). At higher forward biases (when the Fermi level is near the conduction band of the TiO_2, and therefore, the DOS is highly filled) the electron lifetime of devices using **PT-1** is about 10 to 20 times lower (see Figure 7) than with **PT-2** leading to an expected change in V_{oc} of 60 to 78 mV in-between the different devices. The observed difference in V_{oc} for these different external biases at 1 sun illumination is 69 mV; thus, the estimation over the electron lifetime coming from the EIS measurement is in good agreement with the experimentally observed difference in V_{oc}.

In general, **PT-1** shows a high recombination rate, which is clearly observed in the low photovoltage obtained when using this dye in DSSCs. The insertion of the CPDT moiety containing aliphatic side chains leads not only to a spectral response shift toward the red, but also to a retardation of the recombination by more than 10 times. Hence, the strategy of dye design used for **PT-2** indicates a promising approach for future dye engineering so as to obtain NIR region absorbing dyes.

Photoinduced Absorption Spectroscopy. Photoinduced absorption spectroscopy (PIA) is used to locate spectral features corresponding to the oxidized dye absorbance. A quasi-steady-state of the dye is measured under 470 nm excitation and its absorbance difference ($-\Delta T/T$) is reported in Figure 8

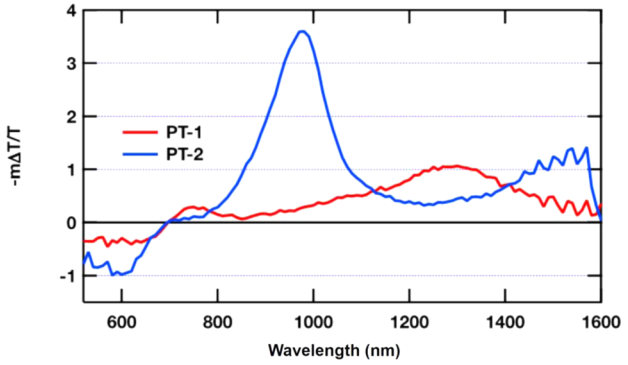

Figure 8. PIA spectra of **PT-1** and **PT-2** dyes anchored onto mesoporous titania in acetonitrile. Excitation wavelength is 470 nm, modulated at 9 Hz.

for dyes **PT-1** and **PT-2** adsorbed onto a mesoporous titania film, immersed in acetonitrile. For both dyes, we observe the bleaching of the dye ground state at 600 nm along with a positive transient absorbance over all the recorded NIR spectra. An isosbestic point between the absorbance of the dye ground and oxidized states is found for both **PT-1** and **PT-2** dyes at 700 nm. It is observed that the introduction of the CPDT group containing the protective alkyl chains not only affects the ground state electronics, but also increases the oxidized state absorbance, with a modification in its absorbance shape. From these data, 1200 nm was chosen as the wavelength to record oxidized dye transient for nanosecond laser flash photolysis experiments.

Transient Absorbance Spectroscopy. Following the observed modifications in the PIA spectra the influence of the CPDT group on the oxidized dye lifetime was scrutinized by nanomicrosecond transient absorbance spectroscopy. After excitation at 605 nm, a change in transient absorbance at 1200 nm was observed as shown in Figure 9. Traces are fitted with a monoexponential function and thus monoexponential lifetimes

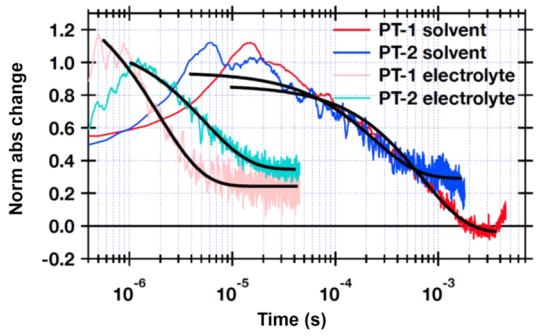

Figure 9. Normalized transient absorbance of **PT-1** and **PT-2** in pure solvent or in electrolyte after excitation at 605 nm, monitored at 1200 nm.

are extracted. In the absence of redox active electrolyte, the oxidized dye can only recombine with the injected electrons in TiO_2 film, and the back electron transfer reaction is monitored. Oxidized **PT-1** has a lifetime of 697 μs. The incorporation of the CPDT unit decreases the lifetime of **PT-2** to 237 μs, indicating a slower recombination between electrons in the TiO_2 with **PT-1** than with **PT-2**.

The regeneration of oxidized dye with a redox active electrolyte (electrolyte composition: 0.03 M I_2, 0.05 M LiI, 0.2 M TBP, 0.1 M GNCS, 1.0 M DMII in acetonitrile and valeronitrile (v/v, 85/15)) is monitored. In this case, faster decay of the oxidized dye is observed, indicating efficient dye regeneration by iodide. This reaction occurs with mono-exponential lifetimes of 1.9 and 5.0 μs for **PT-1** and **PT-2**, respectively. The slower regeneration of**PT-2** is assigned to a more difficult physical access to the dye by the iodide electrolyte due to thesteric hindrance of the alkyl chain substituents on the dye π-bridge. These transient traces do not recover back to zero in this device configurationwithin the measured time frame. Absorbance from electrons in the titanium dioxide conduction band is responsible for this feature, as their lifetime is much longer than the investigated time scale. Assuming a first order rate for both dye regeneration and back electron transfer reactions, we can estimate regeneration yields for both dyes. For **PT-1**, unity regeneration is calculated while calculations yield a 98% regeneration for **PT-2** results. These excellent regeneration yields are mainly attributed to the small steric hindrance coming from the simple indoline donor of these dyes, which allows a facile access to the iodide species in the dye vicinity and, therefore, a fast regeneration lifetime. We conclude from these results that regeneration of this dye by the prepared electrolyte cannot be the limiting step in the operation of devices with **PT-1** or **PT-2** dyes.

CONCLUSION

Two new sensitizers (**PT-1** and **PT-2**) containing [1,2,5]-thiadiazolo[3,4-*c*]pyridine as an acceptor in D-A-π-A organic dyes have been designed and synthesized for use in dye-sensitized solar cells. Incorporating an alkyl cyclopentadithiophene moiety as an additional π-conjugating spacer in the **PT-2** molecule shifts the spectral response to the NIR region and also suppresses the charge recombination rate when compared to the rate observed with the **PT-1** dye. EIS and laser flash photolysis studies show that even though the dye regeneration of **PT-2** dye is slightly lower than that of **PT-1**, the reduced charge recombination rate and enhanced charge collection is

dx.doi.org/10.1021/jp501173b | J. Phys. Chem. C 2014, 118, 17090−17099

responsible for the higher device power conversion efficiency. Our studies clearly demonstrate the relation between sensitizer molecular structure and overall device performance. These findings pave a new path in the design of highly efficient dye sensitizers.

AUTHOR INFORMATION

Corresponding Authors

*E-mail: jlhua@ecust.edu.cn.
*E-mail: shaik.zakeer@epfl.ch.
*E-mail: michael.grätzel@epfl.ch.

Author Contributions

‡These authors contributed equally to this work (J.M. and J.Y.).

Notes

The authors declare no competing financial interest.

ACKNOWLEDGMENTS

This work was supported by NSFC/China (2116110444, 21172073, 91233207 and 21372082) and the National Basic Research 973 Program (2013CB733700). M.G. thanks the Swiss National Science Foundation and European Research Council (ERC) for an Advanced Research Grant (No. 247404) funded under the "Mesolight" Project. J.Y. would like to thank the funding of the visiting program, which is supported by China Scholarship Council (CSC).

REFERENCES

(1) O'Regan, B.; Grätzel, M. A Low Cost High Efficiency Solar Cell Based on Dye Sensitized Colloidal TiO_2 Films. *Nature* **1991**, *353*, 737−740.

(2) Hagfeldt, A.; Boschloo, G.; Sun, L.; Kloo, L.; Pettersson, H. Dye-Sensitized Solar Cells. *Chem. Rev.* **2010**, *110*, 6595−6663.

(3) Zeng, W.; Cao, Y.; Bai, Y.; Wang, Y.; Shi, Y.; Zhang, M.; Wang, F.; Pan, C.; Wang, P. Efficient Dye-Sensitized Solar Cells with an Organic Photosensitizer Featuring Orderly Conjugated Ethylenedioxythiophene and Dithienosilole Blocks. *Chem. Mater.* **2010**, *22*, 1915−1925.

(4) Zhang, M.; Wang, Y.; Xu, M.; Ma, W.; Li, R.; Wang, P. Design of High-Efficiency Organic Dyes for Titania Solar Cells Based on the Chromophoric Core of Cyclopentadithiophene-Benzothiadiazole. *Energy Environ. Sci.* **2013**, *6*, 2944−2949.

(5) Feldt, S. M.; Gibson, E. A.; Gabrielsson, E.; Sun, L.; Boschloo, G.; Hagfeldt, A. Design of Organic Dyes and Cobalt Polypyridine Redox Mediators for High-Efficiency Dye-Sensitized Solar Cells. *J. Am. Chem. Soc.* **2010**, *132*, 16714−16724.

(6) Yella, A.; Lee, H.-W.; Tsao, H. N.; Yi, C.; Chandiran, A. K.; Nazeeruddin, M. K.; Diau, E. W.-G.; Yeh, C.-Y.; Zakeeruddin, S. M.; Grätzel, M. Porphyrin-Sensitized Solar Cells with Cobalt(II/III)-Based Redox Electrolyte Exceed 12% Efficiency. *Science* **2011**, *334*, 629−634.

(7) Yum, J.-H.; Yum, J.-H.; Baranoff, E.; Kessler, F.; Moehl, T.; Ahmad, S.; Bessho, T.; Marchioro, A.; Ghadiri, E.; Moser, J.-E.; et al. A Cobalt Complex Redox Shuttle for Dye-Sensitized Solar Cells with High Open-Circuit Potentials. *Nat. Commun.* **2012**, *3*, 631.

(8) Yum, J.-H.; Walter, P.; Huber, S.; Rentsch, D.; Geiger, T.; Nüesch, F.; Angelis, F. D.; Grätzel, M.; Nazeeruddin, M. K. Efficient Far Red Sensitization of Nanocrystalline TiO_2 Films by an Unsymmetrical Squaraine Dye. *J. Am. Chem. Soc.* **2007**, *129*, 10320−10321.

(9) Mori, S.; Nagata, M.; Nakahata, Y.; Yasuta, K.; Goto, R.; Kimura, M.; Taya, M. Enhancement of Incident Photon-to-Current Conversion Efficiency for Phthalocyanine-Sensitized Solar Cells by 3D Molecular Structuralization. *J. Am. Chem. Soc.* **2010**, *132*, 4054−4055.

(10) Tang, J.; Wu, W.; Hua, J.; Li, J.; Li, X.; Tian, H. Starburst Triphenylamine-Based Cyanine Dye for Efficient Quasi-Solid-State Dye-Sensitized Solar Cells. *Energy Environ. Sci.* **2009**, *2*, 982−990.

(11) Shi, Y.; Hill, R. B. M.; Yum, J.-H.; Dualeh, A.; Barlow, S.; Grätzel, M.; Marder, S. R.; Nazeeruddin, M. K. A High-Efficiency Panchromatic Squaraine Sensitizer for Dye Sensitized Solar Cells. *Angew. Chem., Int. Ed.* **2011**, *50*, 6619−6621.

(12) Delcamp, J. H.; Shi, Y.; Yum, J.-H.; Sajoto, T.; Dell'Orto, E.; Barlow, S.; Nazeeruddin, M. K.; Marder, S. R.; Grätzel, M. The Role of π Bridges in High-Efficiency DSCs Based on Unsymmetrical Squaraines. *Chem.—Eur. J.* **2013**, *19*, 1819−1827.

(13) Richards, C. E.; Anderson, A. Y.; Martiniani, S.; Law, C.; O'Regan, B. C. The Mechanism of Iodine Reduction by TiO_2 Electrons and the Kinetics of Recombination in Dye-Sensitized Solar Cells. *J. Phys. Chem. Lett.* **2012**, *3*, 1980−1984.

(14) Yum, J.-H.; Holcombe, T. W.; Kim, Y.; Rakstys, K.; Moehl, T.; Teuscher, J.; Delcamp, J. H.; Nazeeruddin, M. K.; Grätzel, M. Blue-Coloured Highly Efficient Dye-Sensitized Solar Cells by Implementing the Diketopyrrolopyrrole Chromophore. *Sci. Rep.* **2013**, *3*, 2446.

(15) Blouin, N.; Michaud, A.; Gendron, D.; Wakim, S.; Blair, E.; Neagu-Plesu, R.; Belletête, M.; Durocher, G.; Tao, Y.; Leclerc, M. Toward a Rational Design of Poly(2,7-carbazole) Derivatives for Solar Cells. *J. Am. Chem. Soc.* **2008**, *130*, 732−742.

(16) Sun, Y.; Welch, G. C.; Leong, W. L.; Takacs, C. J.; Bazan, G. C.; Heeger, A. J. Solution-Processed Small-Molecule Solar Cells With 6.7% Efficiency. *Nat. Mater.* **2012**, *11*, 44−48.

(17) Mao, J.; Wang, D.; Liu, S.-H.; Hang, Y.; Xu, Y.; Zhang, Q.; Wu, W.; Chou, P.-T.; Hua, J. Dye-Sensitized Solar Cells Based on Functionally Separated D-π-A Dyes with 2-Cyanopyridine as an Electron-Accepting and Anchoring Group. *Asian J. Org. Chem.* **2014**, *3*, 153−160.

(18) Hua, Y.; Wang, H.; Zhu, X.; Islam, A.; Han, L.; Qin, C.; Wong, W.-Y.; Wong, W.-K. New Simple Panchromatic Dyes Based on Thiadiazolo[3,4-*c*]pyridine Unit for Dye-Sensitized Solar Cells. *Dyes Pigments* **2014**, *102*, 196−203.

(19) Wu, Y.; Zhu, W. Organic Sensitizers from D-π-A to D-A-π-A: Effect of the Internal Electron-Withdrawing Units on Molecular Absorption, Energy Levels and Photovoltaic Performances. *Chem. Soc. Rev.* **2013**, *42*, 2039−2058.

(20) Zhou, D.; Cai, N.; Long, H.; Zhang, M.; Wang, Y.; Wang, P. An Energetic and Kinetic View on Cyclopentadithiophene Dye-Sensitized Solar Cells: The Influence of Fluorine vs Ethyl Substituent. *J. Phys. Chem. C* **2011**, *115*, 3163−3171.

(21) Tsao, H. N.; Yi, C.; Moehl, T.; Yum, J.-H.; Zakeeruddin, S. M.; Nazeeruddin, M. K.; Grätzel, M. Cyclopentadithiophene Bridged Donor-Acceptor Dyes Achieve High Power Conversion Efficiencies in Dye-Sensitized Solar Cells Based on the tris-Cobalt Bipyridine Redox Couple. *ChemSusChem* **2011**, *4*, 591−594.

(22) Qu, S.; Qin, C.; Islam, A.; Wu, Y.; Zhu, W.; Hua, J.; Tian, H.; Han, L. A Novel D-A-π-A Organic Sensitizer Containing a Diketopyrrolopyrrole Unit with a Branched Alkyl Chain for Highly Efficient and Stable Dye-Sensitized Solar Cells. *Chem. Commun.* **2012**, *48*, 6972−6974.

(23) Mao, J.; He, N.; Ning, Z.; Zhang, Q.; Guo, F.; Chen, L.; Wu, W.; Hua, J.; Tian, H. Stable Dyes Containing Double Acceptors without COOH as Anchors for Highly Efficient Dye-Sensitized Solar Cells. *Angew. Chem., Int. Ed.* **2012**, *51*, 9873−9876.

(24) Mao, J.; Guo, F.; Ying, W.; Wu, W.; Li, J.; Hua, J. Benzotriazole-Bridged Sensitizers Containing a Furan Moiety for Dye-Sensitized Solar Cells with High Open-Circuit Voltage Performance. *Chem.—Asian J.* **2012**, *7*, 982−991.

(25) Fabregat-Santiago, F.; Bisquert, J.; Garcia-Belmonte, G.; Boschloo, G.; Hagfeldt, A. Influence of Electrolyte in Transport and Recombination in Dye-Sensitized Solar Cells Studied by Impedance Spectroscopy. *Sol. Energy Mater. Sol. Cells* **2005**, *87*, 117−131.

(26) Fabregat-Santiago, F.; Garcia-Belmonte, G.; Mora-Sero, I.; Bisquert, J. Characterization of Nanostructured Hybrid and Organic Solar Cells by Impedance Spectroscopy. *Phys. Chem. Chem. Phys.* **2011**, *13*, 9083−9118.

(27) Handy, S. T.; Wilson, T.; Muth, A. Disubstituted Pyridines: The Double-Coupling Approach. *J. Org. Chem.* **2007**, *72*, 8496−8500.

(28) Ying, W.; Yang, J.; Wielopolski, M.; Moehl, T.; Moser, J.-E.; Comte, P.; Hua, J.; Zakeeruddin, S. M.; Tian, H.; Grätzel, M. New Pyrido[3,4-*b*]pyrazine-Based Sensitizers for Efficient and Stable Dye-Sensitized Solar Cells. *Chem. Sci.* **2014**, *5*, 206−214.
(29) Zhu, W.; Wu, Y.; Wang, S.; Li, W.; Li, X.; Chen, J.; Wang, Z.; Tian, H. Organic D-A-π-A Solar Cell Sensitizers with Improved Stability and Spectral Response. *Adv. Funct. Mater.* **2011**, *21*, 756−763.
(30) Cai, S.; Tian, G.; Li, X.; Su, J.; Tian, H. Efficient and Stable DSSC Sensitizers Based on Substituted Dihydroindolo[2,3-*b*]carbazole Donors with High Molar Extinction Coefficients. *J. Mater. Chem. A* **2013**, *1*, 11295−11305.
(31) Wang, Z.; Cui, Y.; Dan-oh, Y.; Kasada, C.; Shinpo, A.; Hara, K. Thiophene-Functionalized Coumarin Dye for Efficient Dye-Sensitized Solar Cells: Electron Lifetime Improved by Coadsorption of Deoxycholic Acid. *J. Phys. Chem. C* **2007**, *111*, 7224−7230.
(32) Jie, S.; Chen, J.; Chai, Z.; Wang, H.; Tang, R.; Fan, K.; Wu, M.; Han, H.; Qin, J.; Peng, T.; et al. High Performance Organic Sensitizers Based on 11,12-Bis(hexyloxy) dibenzo[*a*,*c*]phenazine for Dye-Sensitized Solar Cells. *J. Mater. Chem.* **2012**, *22*, 18830−18838.
(33) Hehre, W. J. *Wavefunction*; Wavefunction, Inc.: Irvine, CA.
(34) Marinado, T.; Hagberg, D. P.; Hedlund, M.; Edvinsson, T.; Johansson, E. M. J.; Boschloo, G.; Rensmo, H.; Brinck, T.; Sun, L.; Hagfeldt, A. Rhodanine Dyes for Dye-Sensitized Solar Cells: Spectroscopy, Energy Levels and Photovoltaic Performance. *Phys. Chem. Chem. Phys.* **2009**, *11*, 133−141.
(35) Kuang, D.; Klein, C.; Snaith, H. J.; Moser, J.-E.; Humphry-Baker, R.; Comte, P.; Zakeeruddin, S. M.; Grätzel, M. Ion Coordinating Sensitizer for High Efficiency Mesoscopic Dye-Sensitized Solar Cells: Influence of Lithium Ions on the Photovoltaic Performance of Liquid and Solid-State Cells. *Nano Lett.* **2006**, *6*, 769−773.